Acrylonitrile butadiene styrene (ABS) and polycarbonate (PC) filaments three-dimensional (3-D) printer emissions-induced cell toxicity

Mariana T. Farcas[a,b], Aleksandr B. Stefaniak[c,**], Alycia K. Knepp[c], Lauren Bowers[c],
William K. Mandler[a], Michael Kashon[d], Stephen R. Jackson[e], Todd A. Stueckle[f], Jenifer D. Sisler[a],
Sherri A. Friend[a], Chaolong Qi[g], Duane R. Hammond[g], Treye A. Thomas[h], Joanna Matheson[h],
Vincent Castranova[b], Yong Qian[a,*]

[a] Pathology and Physiology Branch, Health Effects Laboratory Division, National Institute for Occupational Safety and Health, Morgantown, WV, 26505, USA
[b] Pharmaceutical and Pharmacological Sciences, School of Pharmacy, West Virginia University, Morgantown, WV, 26505, USA
[c] Field Studies Branch, Respiratory Health Division, National Institute for Occupational Safety and Health, Morgantown, WV, 26505, USA
[d] Biostatistics and Epidemiology Branch, Health Effects Laboratory Division, National Institute for Occupational Safety and Health, Morgantown, WV, 26505, USA
[e] Exposure Assessment Branch, Health Effects Laboratory Division, National Institute for Occupational Safety and Health, Morgantown, WV, 26505, USA
[f] Allergy and Clinical Immunology Branch, Health Effects Laboratory Division, National Institute for Occupational Safety and Health, Morgantown, WV, 26505, USA
[g] Engineering and Physical Hazards Branch, Division of Applied Research & Technology, National Institute for Occupational Safety and Health, Cincinnati, OH, USA
[h] Office of Hazard Identification and Reduction, U.S. Consumer Product Safety Commission, Rockville, MD, USA

GRAPHICAL ABSTRACT
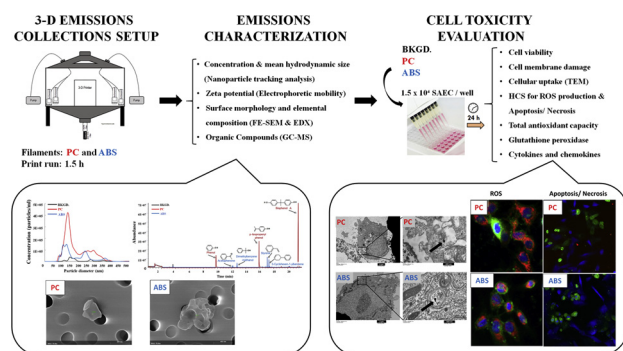
ARTICLE INFO

ABSTRACT

During extrusion of some polymers, fused filament fabrication (FFF) 3-D printers emit billions of particles per minute and numerous organic compounds. The scope of this study was to evaluate FFF 3-D printer emission-induced toxicity in human small airway epithelial cells (SAEC). Emissions were generated from a commercially available 3-D printer inside a chamber, while operating for 1.5 h with acrylonitrile butadiene styrene (ABS) or polycarbonate (PC) filaments, and collected in cell culture medium. Characterization of the culture medium

* Corresponding author at: Pathology and Physiology Branch, Health Effects Laboratory Division, National Institute for Occupational Safety and Health, 1095 Willowdale Road, Morgantown, WV, 26505, USA.
** Corresponding author at: Respiratory Health Division, National Institute for Occupational Safety and Health, Morgantown, 1095, Willowdale Road, Morgantown, WV, 26505, USA.
E-mail addresses: woe7@cdc.gov (M.T. Farcas), boq9@cdc.gov (A.B. Stefaniak), ydt0@cdc.gov (A.K. Knepp), mju3@cdc.gov (L. Bowers),
oex1@cdc.gov (W.K. Mandler), mqk1@cdc.gov (M. Kashon), yif8@cdc.gov (S.R. Jackson), jux5@cdc.gov (T.A. Stueckle), sislerj@gmail.com (J.D. Sisler),
shf8@cdc.gov (S.A. Friend), hif1@cdc.gov (C. Qi), ahz0@cdc.gov (D.R. Hammond), tthomas@cpsc.gov (T.A. Thomas), jmatheson@cpsc.gov (J. Matheson),
vcastran@hsc.wvu.edu (V. Castranova), yaq2@cdc.gov (Y. Qian).

revealed that repeat print runs with an identical filament yield various amounts of particles and organic compounds. Mean particle sizes in cell culture medium were 201 ± 18 nm and 202 ± 8 nm for PC and ABS, respectively. At 24 h post-exposure, both PC and ABS emissions induced a dose dependent significant cytotoxicity, oxidative stress, apoptosis, necrosis, and production of pro-inflammatory cytokines and chemokines in SAEC. Though the emissions may not completely represent all possible exposure scenarios, this study indicate that the FFF could induce toxicological effects. Further studies are needed to quantify the detected chemicals in the emissions and their corresponding toxicological effects.

1. Introduction

Additive manufacturing (AM) is a family of processes used to build physical objects from a computer-aided design model. Fused filament fabrication (FFF) is a type of material extrusion technology used by some 3-D printers to melt and extrude a thermoplastic filament through a heated nozzle to deposit material on a plate, layer-by-layer, to create a physical object. 3-D printing provides a novel approach for the fabrication of intricate items that can potentially combine optical, chemical, electronic, electromagnetic, fluidic, thermal and acoustic features (Xu et al., 2017). Some of the uses of 3-D printing include tissue and organ fabrication; creating prosthetics, implants, and anatomical models; pharmaceutical research concerning drug discovery, delivery, and dosage forms; parts for motor vehicles and rocket engines; and devices in various industries to advance innovation, production, and efficiency. The U.S. 3-D printing market is anticipated to grow at a compound annual growth rate of 27% by 2024, and it is expected to exceed more than a $7 billion industry in the U.S. over this time (MarketResearchEngine, 2018).

The feedstock materials used in AM systems can be liquid or solid in the form of plastics, metals, or ceramics. Plastics used in FFF 3-D printer filaments may also include infill materials, such as wood fiber, carbon fiber, silica, or engineered nanomaterials (*e.g.*, multi-walled carbon nanotubes). Several types of feedstock filaments are commercially available for use in FFF 3-D printers including, but not limited to, polycarbonate (PC) and acrylonitrile butadiene styrene (ABS). Previous studies have shown that: 1) thermal degradation of these filaments during 3-D printing releases fine and ultrafine particles; 2) average particle emission rates range from $\sim 10^8$ to $\sim 10^{11}$ particles/min with some variances among different types and brands of filaments and within same filaments, but different colors; and 3) particle emission rates fluctuate over the course of printing, with the highest emission rates occurring at the beginning of printing (Azimi et al., 2016; Deng et al., 2016; Floyd et al., 2017; Gu et al., 2019; Kim et al., 2015; Stabile et al., 2017; Stefaniak et al., 2017b; Steinle, 2016; Stephens et al., 2013; Vance et al., 2017; Wojtyła et al., 2017; Yi et al., 2016; Zhang et al., 2017; Zhou et al., 2015). In addition to particles, FFF 3-D printers also emit numerous volatile, semi-volatile, and non-volatile organic compounds during thermal processing, such as: aldehydes, ketones, alcohols, aromatics (benzene, toluene, ethylbenzene, xylenes, styrene), and phthalates (Kim et al., 2015; Stefaniak et al., 2017b).

Several recent studies have shown that exposure to 3-D printer-emissions can induce potential toxic effects in both humans and animals (House et al., 2017; Macdonald et al., 2016; Oskui et al., 2016; Stefaniak et al., 2017a). A case report showed that a businessman who operated 3-D printers using ABS feedstock in a small work area of approximately 85 m³ developed work-related asthma within 10 days of initial exposure (House et al., 2017). In a human exposure study, volunteers were exposed to emissions from a desktop 3-D printer for 1 h, followed by assessing changes in acute inflammatory biomarkers (Gumperlein et al., 2018). Although no clinically significant acute changes in the biochemical responses of nasal secretions and urine were found, the volunteers' exhaled air showed increased levels of nitric oxide, which might be due to inhaled ultrafine particle-induced eosinophilic inflammation (Gumperlein et al., 2018). Exposure of zebrafish embryos to 3-D printer raw materials has been found to affect their

survival and hatching rates, resulting in the inhibition of embryo development, estrogen receptor transactivation, and oocyte maturation (de Almeida Monteiro Melo Ferraz et al., 2018; Macdonald et al., 2016; Oskui et al., 2016). Stefaniak et al. (2017a) investigated the acute toxic effects of ABS 3-D printer emissions on cardiovascular function, after nose-only inhalation exposure in rats. It was found that the exposure to these emissions for 3 h induced significantly higher mean arterial pressure concomitant with elevated resting arteriolar tone and impaired endothelium-dependent arteriolar dilation (Stefaniak et al., 2017a).

Considering the fast-growing application of 3-D printing technology, the reported emissions, and the potential adverse health effects from exposure to these emissions, there is a need to study the toxicity of 3-D printer emissions and the mechanisms of toxicity both *in vivo* and *in vitro*. In this study, emissions were generated in a 0.62 m³ environmental chamber using a commercially available FFF 3-D printer using PC or ABS filaments. The emissions were collected in serum-free cell culture medium and characterized to determine the mean hydrodynamic particle size (nm), particle concentration (particles/mL), zeta potential, and small organic molecule content. Human small airway epithelial cells (SAEC) were exposed to these emissions in cell culture medium to investigate cytotoxicity, apoptosis, and oxidative stress and inflammatory markers at 24 h post exposure.

2. Materials and methods

2.1. Emissions collection setup

The 3-D printer emissions were collected in a stainless-steel test chamber (TSE Systems, Chesterfield, MO). The collection system consisted of: 1) a 0.62 m³ stainless-steel chamber to house a desktop 3-D printer (LulzBot Mini, Aleph Objects, Inc., Loveland, CO); 2) a laptop computer located outside of the chamber to control printer operation; 3) four BioSamplers® (SKC, Inc., Eighty Four, PA) containing 20 mL of Small Airway Epithelial Cell Basal Medium (SABM™) (Lonza Inc., Allendale, NJ) (located inside of the chamber at a distance of 20–25 cm from the printer); and 4) tubing that connected the BioSamplers® to high flow pumps (located outside the chamber) to sample chamber air at 12.5 L/min (*via* sonic orifices in the BioSamplers®). The purpose of the chamber was to collect sufficient amounts of emissions for the planned *in vitro* studies in a reasonable time period. As such, the chamber volume is smaller than a typical room where a 3-D printer may be operated; however, the distance from the BioSampler® inlet to the printer is reasonable based on our experiences performing workplace assessments. Each BioSampler® consists of an inlet section, a nozzle section containing three nozzles, and a collection section containing SABM™. The three sampler components are connected by a fritted glass fitting. When connected, the three nozzles are positioned above SABM™ in the collection vessel and airflow through these nozzles (flow rate controlled by sonic orifices) creates a vortex. As air is drawn through the nozzles, particles and vapors in chamber air are trapped in the SABM™. To minimize evaporation of the cell culture medium, two BioSamplers® were operated for the first 45 min of the print job and two BioSamplers® were operated during the last 45 min of the print job. Upon completion of sampling, each BioSampler® (each containing about 10 mL of unevaporated media) was rinsed with a few milliliters of fresh media, and the contents from all four BioSamplers® were

combined in order to obtain an approximately 50 mL sample that was representative of emissions from the entire 1.5-h print job. In preliminary studies performed to evaluate potential effect of temperature on emissions collection, chamber air was sampled using BioSamplers® placed in ice baths or at room temperature; no difference was observed in collected emissions characteristics between the two methods. A two-piece high efficiency particulate air filter and activated carbon filter (Whatman, Maidstone, UK) was attached to the chamber inlet to remove particles and organic chemicals, respectively, from the ambient air before it entered the chamber. The chamber has sampling ports through which sampling tubing was inserted to connect to the high flow pumps (Supplemental Fig. S1 illustrates the sampling setup). The 3-D printer sat on an approximately 100 cm x 60 cm perforated stainless-steel support plate to allow for upward airflow inside the chamber. This minimized areas of stagnant air in the chamber and resulted in 3-D printer emissions being distributed uniformly in this chamber; thereby, minimizing bias relative to sampling positions. The chamber leak rate and air exchange rate were determined by dosing the chamber with sulfur hexafluoride (SF_6) and monitoring its concentration using an infrared spectrophotometer (Miran Sapphire, Thermo Scientific, Waltham, MA). The leak rate over an eight-hour period was found to be 0.8%, and the air-change rate was 2.42 air changes per hour (ASTM-D6670, 2013; ISO.28360, 2007).

Black PC (Gizmo Dorks LLC, Temple City, CA) and black ABS (3DXTech, Byron Center, MI) filaments were used to 3-D print an artifact designed by the National Institute of Standards and Technology (NIST) (Moylan et al., 2014). Printer settings were 240 °C/110 °C (extruder nozzle temp/printer bed temp) and 290 °C/110 °C for ABS and PC, respectively (as recommended by manufacturers). The NIST artifact was printed three times using PC filament (runs designated PC1, PC2, and PC3) and three times using ABS filament (runs designated ABS1, ABS2, and ABS3) and was scaled to print within 1.5 h. A background sample was also collected for 1.5 h by sampling chamber air, while the 3-D printer was inside the chamber but powered off and not operating. After printing, aliquots of culture media were taken from the samples for characterization (described below). The remainder of the medium was stored at 4 °C in a sterile glass bottle and used for *in vitro* toxicity assessment within 24–36 h.

2.2. Emissions characterization

2.2.1. Particle size and concentration in cell culture medium

Mean hydrodynamic particle size and particle concentration were determined using nanoparticle tracking analysis (NTA) (NanoSight NS300, Malvern Instruments, Worcestershire, UK). For analysis, a syringe pump was used to inject all samples through a Low Volume Flow Cell top plate at a constant rate at room temperature. Camera and threshold settings in the NTA instrument varied slightly with each sample to ensure accurate particle characterization. SABM™ and background samples were also ran at camera levels/threshold settings similar to the ABS and PC printing samples in an effort to determine how much the SABM™ and ambient air contributed to the NTA measurements. Each sample was captured five times for 60 s, for a total capture time of 5 min per sample.

Zeta potential was determined by electrophoretic light scattering (ELS) using a Zetasizer Nano ZS90 (Malvern Instruments, Worcestershire, UK). The pH of each sample was measured before each run using a SevenMulti calibrated electrode (Mettler-Toledo, LLC, Columbus, OH). The parameters of all runs were as follows: refractive index of material = 0.100, absorbance of material = 0.100, refractive index of dispersant = 1.334, viscosity of dispersant = 0.9110 cP, dielectric constant = 80.2, and temperature = 25 °C.

2.2.2. Morphology and elemental composition of particles in medium

Particles collected in cell culture medium were filtered onto a 0.2-micron polycarbonate filter, mounted on a clean aluminum sampling

stub, and coated with a thin layer of gold/palladium. Particles collected on the filters were imaged and analyzed using a field emission – scanning electron microscope (FE-SEM, Hitachi S-4800, Tokyo, Japan) equipped with an energy dispersive x-ray detector (EDX, Quantax, Bruker Scientific Instruments, Berlin, Germany) to determine elemental contents.

2.2.3. Analysis of organic compounds collected in the cell culture medium

Samples were stored at 4 °C until ready for analysis when they were brought to room temperature. An unfiltered 2-mL aliquot was sampled by submerging a polydimethylsiloxane/divinylbenzene (PDMS/DVB) (65 μm film thickness) solid-phase microextraction (SPME) fiber in the solution for one hour. After one hour, the SPME fiber was removed, and the sample was analyzed by gas chromatography-mass spectrometry (GC–MS). The inlet temperature was at 250 °C in splitless mode. The GC–MS was operated in constant flow mode at 1.2 mL/min with ultra-high purity grade helium as the carrier gas. Separation occurred using an HP-5MS column and the following oven program: 40 °C for 6 min, ramp to 80 °C at 20 °C/min, hold 4 min, ramp to 240 °C at 20 °C/ min, hold 2 min. Compounds were tentatively identified by comparing mass spectra to the 2014 NIST/EPA/NIH Mass Spectral Library (NIST 14); only compounds that matched ≥70% with the Library are reported herein.

2.3. In vitro toxicity evaluation of collected 3-D printer emissions

2.3.1. Quantitation of endotoxin

Potential endotoxin contamination was examined using Pierce™ LAL Chromogenic Endotoxin Quantitation Kit (Thermo Scientific, Waltham, MA). A standard curve representing endotoxin unit/ mL (EU/ mL) was created using *E. coli* endotoxin as a standard, according to the manufacturer's instructions. The level of endotoxin for all samples was similar to the endotoxin-free water sample, which was less than 0.05 EU/ mL (approx. 0.005 ng/ mL).

2.3.2. Cell culture

Human SAEC were obtained from Dr. Tom K. Hei's laboratory (Piao et al., 2005) at Columbia University (New York, NY, USA) and maintained in SABM™ supplemented with the Small Airway Epithelial Growth Medium (SAGM™) BulletKit, at 37 °C with 5% CO_2, according to the manufacturer's instructions (Lonza Inc., Allendale, NJ).

To assess cytotoxicity, oxidative stress response, apoptotic effects and cytokine production, SAEC were seeded in 96-well plates at a density of 1.5×10^4 cells per well overnight, followed by serum-starvation for 12 h. This was done to model an epithelial monolayer response. Next, SAEC were exposed for 24 h to 100 μL/ well of medium containing PC or ABS emissions. Each PC (prints 2 and 3) and ABS (prints 2 and 3) emissions collected in medium were mixed by vigorous vortexing for 5 min, and exposed as undiluted (0%), 25% dilution, and 50% dilution in serum-free SABM™, resulting in six doses for each filament type (Supplemental Table S1). For cellular uptake and cell morphology evaluation, SAEC were seeded in 6-well plates at a density of 0.5×10^6 cells per well overnight, followed by exposure to undiluted 3-D printer emissions in 2 mL cell culture medium for 24 h. The background sample was used undiluted. The control samples were treated with SABM™.

2.3.3. Cell viability assay

Cellular viability was determined using the AlamarBlue bioassay according to the manufacturer's instructions (ThermoFischer Scientific, Waltham, MA). Briefly, at 24 h post exposure, the supernatants were collected for the measurements of lactate dehydrogenase (LDH), along with cytokine and chemokines release. The cells were rinsed with 100 μL SABM™/ well once, followed by addition of 200 μL of 10% AlamarBlue solution to each well. After 4 h incubation at 37 °C, the viability was measured by quantifying fluorescence levels (ex/em 560/

590 nm) using the Synergy H1 hybrid multi-mode microplate reader (BioTek Instruments, Inc., Winooski, VT).

2.3.4. Cell membrane damage

The release of LDH into the cell-free supernatants was assayed spectrophotometrically by monitoring the reduction of nicotinamide adenine dinucleotide at 340 nm in the presence of lactate using a Lactate Dehydrogenase Reagent Set (Pointe Scientific, Inc., Lincoln Park, MI).

2.3.5. Transmission electron microscopy

To evaluate the cellular uptake of particles and morphological changes, exposed SAEC were washed with HEPES Buffered Saline solution and detached using Trypsin/EDTA Solution (Reagent Pack™ Subculture Reagents, Lonza). After cells were released, the trypsin was neutralized with Trypsin Neutralizing Solution (Lonza) and harvested by centrifugation at 800 × rpm for 5 min at room temperature, followed by fixation in Karnovsky's fixative (2.5% glutaraldehyde, 2.5% paraformaldehyde in 0.1 M Sodium Cacodylic buffer). Then, the cells were post-fixed in osmium tetroxide, mordanted in 1% tannic acid and stained *en bloc* in 0.5% uranyl acetate. The samples were embedded in epon™ (epoxy resin in xylene), sectioned and stained with 4% uranyl acetate and Reynold's lead citrate. The sections were imaged on a JEOL 1400 transmission electron microscope (JEOL, Tokyo, Japan).

2.3.6. Biomarkers of oxidative stress in cell lysates

Oxidative damage was evaluated using Total Antioxidant Capacity (TAC) and Glutathione Peroxidase (GPx) assay kits (Abcam, Cambridge, CA) with minor modifications. After the conditioned media were collected, the cells were re-suspended in 50 μL MilliQ water and 100 μL assay buffer, respectively, and stored at -80 °C for 24 h to induce lysis. Upon thawing, the plates were vigorously shaken at 900 rpm for 5 min, followed by pipetting up and down three times, and then transferred into the test tubes. Both assays were performed according to the manufacturer's instructions. The results were normalized to total protein concentrations determined using Pierce™ BCA Protein Assay (ThermoFisher Scientific, Waltham, MA).

2.3.7. High content screening

2.3.7.1. Reactive oxygen species (ROS) production.
For high content screening (HCS), live cells were stained with a cocktail consisting of 5 μM CellROX™ Deep Red reagent, 5 μg/ mL of CellMask™ Green plasma membrane stain, and 1 μM Hoechst 33342 fluorescent nuclear stain (Thermo Fisher Scientific, Waltham, MA) in culture medium, and incubated for 30 min at 37 °C. Next, the plates were washed two times with warm HEPES Buffered Saline Solution (Lonza) and imaged immediately on an ImageXpress Micro XLS (IMX) system (Molecular Devices, Sunnyvale, CA). Nine sites per well were imaged at 20X magnification with a CMOS 16-bit digital camera using Cy5 (ex/em

628/692 nm), TRITC (ex/em 543/593 nm), and DAPI (ex/em 377/447 nm) filter cubes. Images from HCS assays were analyzed with the MultiWavelenth Application Module in MetaXpress v5.3 software to determine mean ROS intensity (Chambers et al., 2018). Briefly, masks were applied to cell nuclei, plasma membrane staining, and ROS signal by user-defined parameters including minimum width, maximum width, minimum intensity above background, and minimum area stained. Only those positively stained masks that contained a nucleus were scored as a cell. Mean integrated intensity of cellular ROS stain was calculated for each site by determining stain intensity under the area of each mask divided by the number of cells in each image. Mean intensities were then averaged within and across replicates.

2.3.7.2. Apoptosis and necrosis.
The apoptotic and necrotic cells were determined using Cell Meter™ Apoptotic and Necrotic Multiplexing Detection kit (AAT Bioquest, Inc., Sunnyvale, CA) according to the manufacturer's instructions. Briefly, at 24 h post-exposure, a cocktail consisting of 2 μL of Apopxin™ Red apoptosis stain, 1 μL of 200X Nuclear Green™ DCS1 necrotic stain, and 1 μL of CytoCalcein™ Violet 450 cytoplasmic stain was added to each well in culture medium and incubated for 30 min at 37 °C. Next, the plates were washed two times with warm HEPES Buffered Saline Solution and imaged immediately on the IMX system. Apopxin™ Deep Red staining on the plasma membrane indicated dye binding to phosphatidylserine, an indicator of the apoptosis. Nine sites per well were imaged at 10X magnification using Cy5, FITC (ex/em 470/525 nm), and DAPI filter cubes. To analyze the images, masks were applied using minimum/maximum diameters, and minimum intensities for each channel as described above. Apoptotic cells appeared red and green + red, the necrotic cells were green, and viable cells appeared blue only. Cell counts and percentages for each phenotype at each site were calculated and averaged within and across replicates.

2.3.8. Cytokines, chemokines, and growth factors

The levels of IL-1β, IL-6, IL-8, TNF-α, IL-12/IL-23p40, IL-16, IL-1α, and IL-13 in the cell-free supernatants were determined using V-PLEX Cytokine and Chemokines Human Kits from Meso Scale Discovery (MSD, Meso Scale Discovery). Plates were read using MSD QuickPlex SQ 120 (Meso Scale Discovery) for electrochemiluminescence. Sample concentrations were derived from a standard curve plotted using a four-parameter logistic fit using MSD Workbench software. Data were normalized to total cell number per well determined using HCS.

2.4. Statistics

Studies were performed in three independent experiments with 3–6 replicates each. The data are represented as percent of control. All statistical analyses were performed in either SAS v9.4, or JMP v13. Mixed model regression analyses were performed on the measured
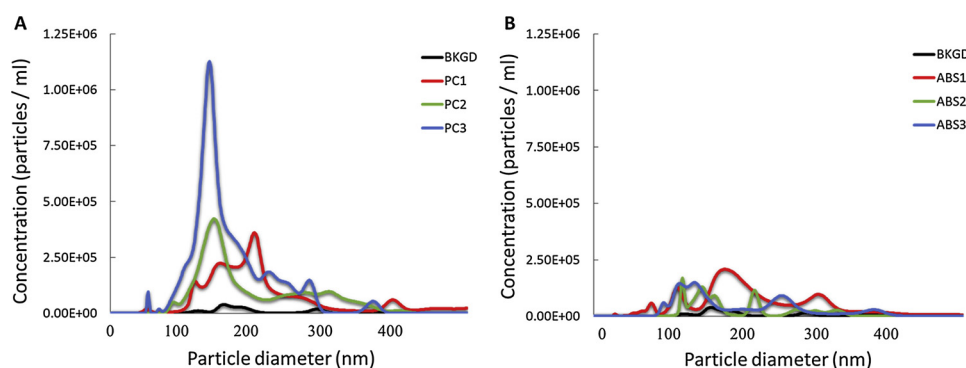
Fig. 1. Number-based size distribution of 3-D printer-emitted particles collected in the cell culture medium. 3-D printer emissions using PC (A) and ABS (B) were collected in cell culture medium, followed by analysis using NTA.
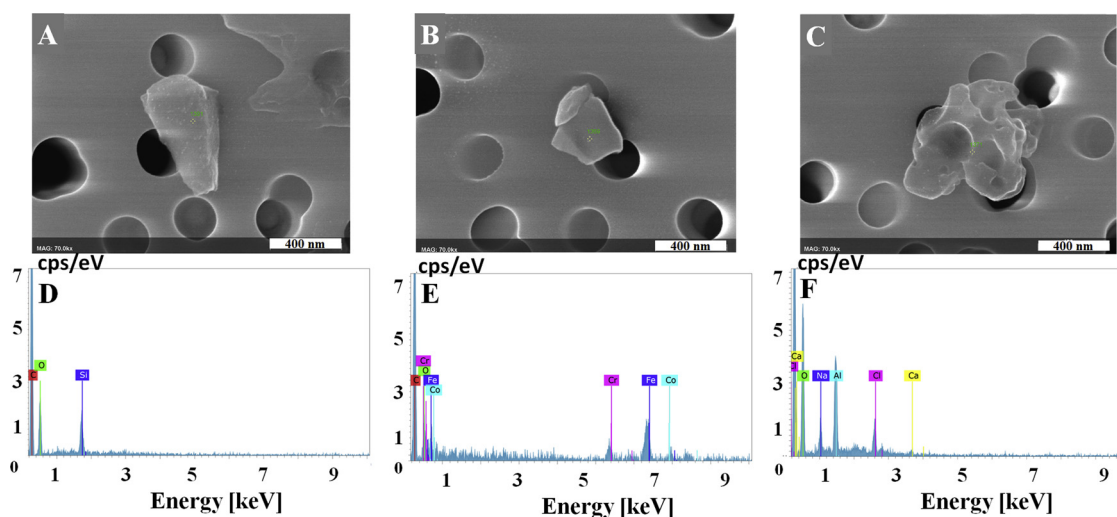
Fig. 2. Representative images of 3-D printer-emitted particles collected in the cell culture medium indicating surface morphology and elemental composition. 3-D printer emissions were collected in cell culture medium, passed through a track-etched polycarbonate filter, and analyzed using FE-SEM (A–C) and EDX (D–F). (A) Background, (B) PC, (C) ABS. D–F are representative elemental analysis spectra for A–C. Magnification at 70k × for all images, scale bar at 400 nm.

variables using particle number*10^{-4} as the independent variable, and printer batch as a random factor. These analyses included background levels of particles as data points, as well as zero particle controls. Regression coefficients which are significantly different from 0, indicate dose-responsiveness of the dependent variables. Analyses were performed for the two filaments separately. All analyses are considered significant at $p < 0.05$.

3. Results

3.1. Physicochemical characterization of FFF 3-D printer emissions in cell culture medium

3-D printer emissions were collected in SABM™ and characterized to determine particle concentration, mean hydrodynamic diameter size, zeta potential, particle morphology, and organic compounds content. Supplemental Table S2 presents characteristics of the SABM™ medium for the PC and ABS print runs. The printing of both filaments resulted in higher numbers of particles in cell culture medium compared to the background air control. Note that the "background" sample was collected by pulling chamber air through the BioSamplers® with SABM media while the 3-D printer was off. The background particle counts in media may be from: 1) particles in the chamber or in chamber air that passed through the HEPA-filtered make-up air (usually < 500 particles/cm³); 2) solids in the culture media; and/or, 3) air bubbles formed during sampling from agitation and swirling of the media in the BioSampler®. During extrusion of ABS and PC, peak particle number concentrations are 10^4 to 10^5 particles/cm³ (Stefaniak et al., 2018; Yi et al., 2016) meaning that the contribution of ambient particles to printer emitted particles is at most 5%. NTA of media (no air pulled through it) confirmed that the media contained virtually no particles indicating that there were no solids in the media that were incorrectly counted as particles. Hence, the background "particle" concentration in the SABM media presented in Table S2 consists of a small fraction of ambient dust particles but the majority of "particle" counts were likely an artifact from the instrument sensing air bubbles formed by agitation and swirling of media while drawing air through the BioSamplers®. PC filament led to a higher number of particles compared with ABS. The mean diameters of particles of PC and ABS in the medium were 201 ± 18 nm and 202 ± 8 nm, respectively. The zeta potentials of particles in both suspensions were negative, about −18 mV. The number-based size distribution of the particles showed that the PC run had mainly one large distinct mode between 140–170 nm, while ABS

run had two modes, the first at about 140–150 nm and the second at around 250–300 nm, suggesting that particles from ABS had a broader distribution than those from PC (Fig. 1). Representative images of 3-D printer emissions particles collected in cell culture medium indicating surface morphology (FE-SEM) and elemental composition (EDX) are shown in Fig. 2. Occasionally particles composed of silicon were observed on the background filter that may be from the low level of particles in the filtered make-up air or a contaminant on the filter. The morphology of the background particle was more angular than the printer emitted particles and its elemental composition was consistent with ambient dust and dissimilar from the printer emitted particles. EDX analysis showed that the main elements of PC and ABS particles were C, O, Ca, Na, Si, Ni, Cr, Fe, S, Al, and Cl (Fig. 2).

SPME/GC–MS was used to identify the organic compounds in the collected emission medium. The results were compared with the NIST/EPA/NIH Mass Spectral Library, and the compounds that matched ≥ 70% with the library are shown in Fig. S2. Supplemental Table S3 shows for information only the qualitative results of the detected individual compounds from all print runs. Representative chromatograms in Fig. S2 show the retention times for each compound identified during the PC an ABS print runs (no organic compounds were detected in the background sample). During the PC print run, the compounds observed in sample collection medium were tentatively identified as bisphenol A (BPA), p-isopropenylphenol, and phenol; whereas, styrene, 3-cyclohexen-1-ylbenzene, α,α-dimethylbenzenemethanol, and acetophenone were detected when the ABS filament was used.

3.2. Toxicological evaluation of 3-D printer emissions collected in media

3.2.1. Uptake of 3-D printer-emitted particles by SAEC

The uptake of particles in the medium by SAEC was investigated. The cells were cultured to confluence in 6-well plates and then were exposed to PC or ABS emissions in suspension, followed by TEM analysis. Fig. 3 presents TEM images indicating the internalization of PC and ABS 3-D printer-emitted particles that were enclosed in a lipid membrane, similar to an endosome.

3.2.2. Cytotoxicity

Both cell viability assays and LDH measurements were performed to determine cellular toxicity from exposure to emissions collected in media. The AlamarBlue-based cell viability assay revealed changes in cell proliferation, while the LDH measurements in the supernatants showed the release of a soluble cytosolic enzyme upon cell death due to
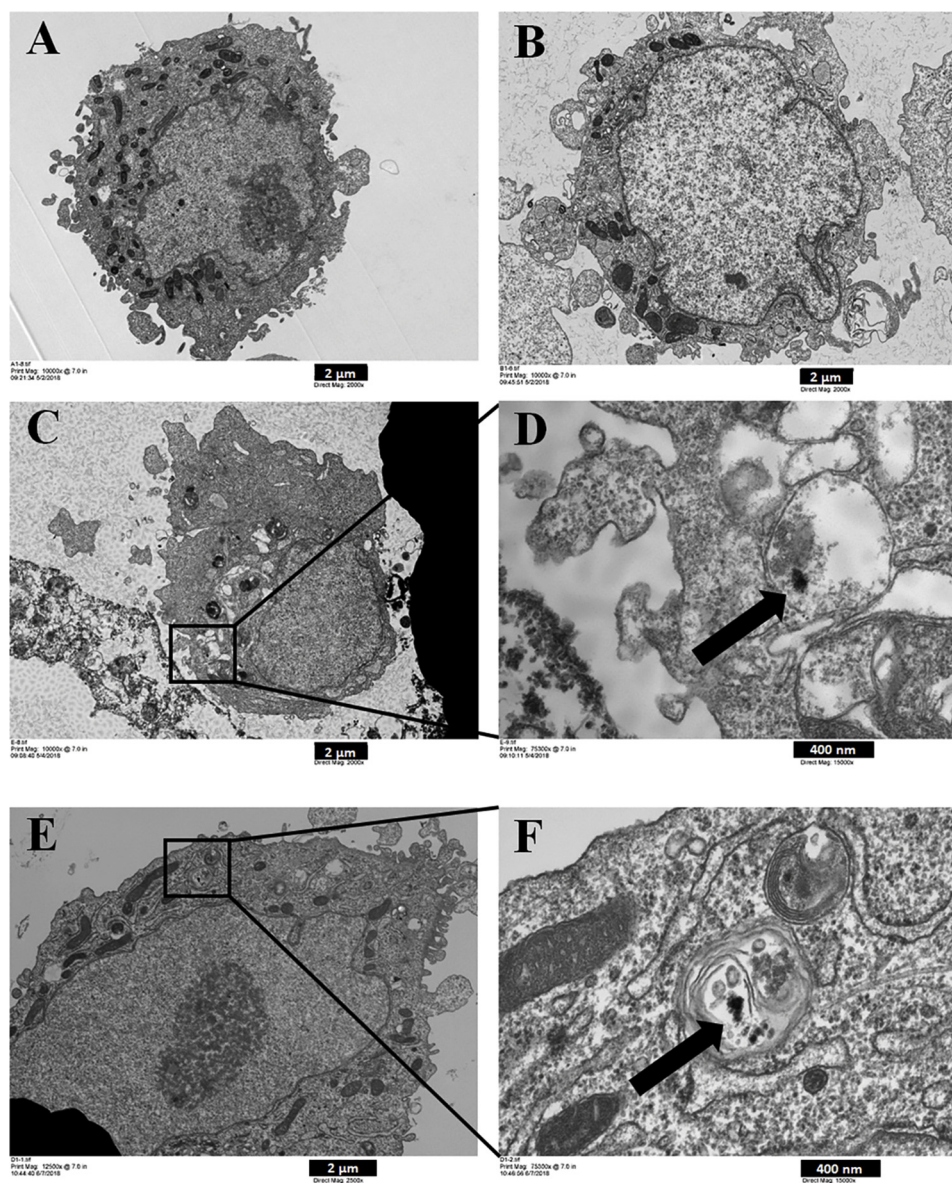
Fig. 3. Uptake by SAEC of 3-D printer-emitted particles collected in the cell culture medium. SAEC were treated with medium containing 3-D printer emissions for 24 h, followed by TEM image analysis. (A) Control, (B) Background, (C) 100% PC, (D) C inset, (E) 100% ABS, and (F) E inset. A, B, and C images are at 2,000x magnification, and image E at 2,500x magnification. D and F images are at 15,000x magnification. A, B, C, and E scale bar at 2 μm; D, F scale bar at 400 nm.

cell membrane damage. 3-D printer emitted particles collected in media induced a significant (p < 0.0001) dose-dependent decrease in cell proliferation (Fig. 4, Table 1). Results revealed that for each 10^4 PC and ABS particle exposure, the cell viability decreased by 0.048% (Table 1). The decrease of cell viability correlated with the dose-dependent increase in LDH activity (p < 0.0001) in the supernatants. Specifically, each 10^4 PC and ABS particle exposure resulted in a significant dose-dependent increase by 0.051% and 0.110% LDH levels in SAEC, respectively (Fig. 4, Table 1). Taken together, these results demonstrate that exposure to both PC and ABS emissions collected in cell culture medium showed a dose–dependent toxicity in SAEC.

3.2.3. ROS production and oxidative stress

It has been well-established that exposure to particulate matter induces the production of ROS, which causes cell injury or oxidative stress, leading to the development of various diseases (Lodovici and Bigagli, 2011; Xia et al., 2006). SAEC were exposed to PC or ABS 3-D printer emissions collected in cell culture medium for 24 h, followed by high content imaging to determine the production of ROS. Both PC and

ABS particles induced a significant (p < 0.0001) dose-dependent increase in the production of ROS (Fig. 5, Table 1). The mixed model regression analyses revealed that for each 10^4 particle exposure, the production of ROS increased by 0.075% and 0.148% for PC and ABS in SAEC, respectively (Table 1).

One of the main properties of ROS is to cause cellular injury, and cellular systems are protected from ROS-induced injury by an array of anti-oxidant defenses. Measurements of TAC and GPx activity can indirectly reflect ROS-induced oxidative stress in cells. As shown in Fig. 6, PC and ABS emitted-particles collected in cell culture medium triggered a significant dose-dependent decrease (p < 0.0001) in TAC levels, with concomitant decline in GPx activity (Table 1). Specifically, for each 10^4 particle exposure, the TAC levels decreased by 0.007% and 0.039% for PC and ABS in SAEC, respectively; whereas the GPx activities decreased by 0.016% and 0.035% for PC and ABS in SAEC, respectively (Table 1).

3.2.4. Apoptosis and necrosis

To confirm apoptosis from exposure to PC emissions collected in media, the measurement of externalization of phosphatidylserine, a
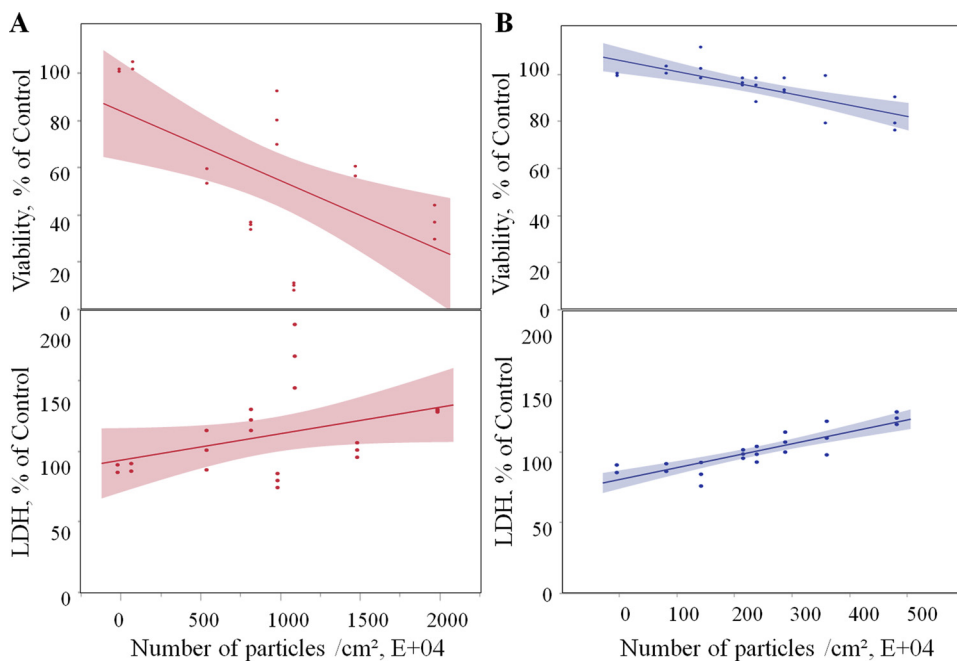
Fig. 4. Cytotoxicity of the 3-D printer-emitted particles collected in the cell culture medium: cell viability and LDH activity following exposure to PC (A) and ABS (B) emissions. Experiments were performed in three independent experiments with n = 6 replicates each. The regressions lines illustrate a significantly ($p < 0.0001$) decreased dose-response relationship between cell proliferation and the numbers of the PC and ABS 3-D printer-emitted particles, which correlated with a significant ($p < 0.0001$) dose-dependent increase in the LDH activity in the supernatants. The shaded area represents the 95% confidence interval around the regression line.

Table 1

Linear regression slopes (with standard errors) of the all variable investigated following exposure to PC and ABS 3-D printer-emitted particles collected in the cell culture medium. All statistical analyses were performed in either SAS v9.4, or JMP v13. Mixed model regression analyses were performed on the measured variables using particle number$*10^{-4}$ as the independent variable, and printer batch as a random factor. Regressions coefficients which are significantly different from 0, indicate dose-responsiveness of the dependent variables. Analyses were performed for the two filaments separately. All analyses are considered significant at $p < 0.05$ (*).

Variable	PC		ABS	
	Slope	StdErr	Slope	StdErr
Viability, % of Control	−0.04790*	0.00319	−0.04794*	0.00733
LDH, % of Control	0.05077*	0.00636	0.11021*	0.00852
ROS, % of Control	0.07479*	0.00960	0.14836*	0.01950
TAC, % of Control	−0.00657*	0.00233	−0.03915*	0.00847
GPx, % of Control	−0.01604*	0.00133	−0.03511*	0.00690
Apoptosis, % of Control	0.28506*	0.05598	0.37508*	0.05277
Necrosis, % of Control	0.23467*	0.03618	0.14447*	0.03246
IL-12p70, pg/total cells	0.00650*	0.00111	0.00760*	0.00112
IL-13, pg/total cells	0.00020*	0.00004	0.00022*	0.00003
IL-16, pg/total cells	0.12797*	0.02741	0.09414*	0.00960
IL-1β, pg/total cells	0.09851*	0.03645	0.00125*	0.00017
IL-1α, pg/total cells	0.01725*	0.00543	0.00268*	0.00081
IL-6, pg/total cells	0.00001*	0.00000	0.00002*	0.00000
IL-8, pg/total cells	0.00095*	0.00018	0.00005	0.00015
TNF-α, pg/total cells	0.00619*	0.00119	0.00064	0.00038

hallmark of apoptosis, was applied. Results illustrated that for each 10^4 PC and ABS exposure, the number of apoptotic cells increases by 0.235% and 0.144% in SAEC, respectively (Table 1). To further identify other mechanism-involved cell death, 7-amino actinomycin D (7-AAD), a membrane impermeant dye which is bound to double-stranded DNA of non-viable cells and excluded from viable cells, was used to determine necrosis upon exposure to emissions collected in media. Results reveal significantly increased dose-response relationship ($p < 0.0001$) between apoptotic or necrotic events and the numbers of the PC and ABS 3-D printer-emitted particles collected in the cell culture medium (Fig. 7, Table 1). Results showed that for each 10^4 PC and ABS particles, the number of necrotic cells increases by 0.285% and 0.375% in SAEC, respectively (Table 1).

### 3.2.5. Cytokine and chemokine responses

A panel of 8 pro-inflammatory cytokines and chemokines in the supernatants was evaluated to determine the inflammatory responses upon exposure to 3-D printer-emitted particles collected in medium and exposed to SAEC. With the exception of IL-8 and TNF-α in the collected ABS emissions-exposed cells, model regressions analysis (Table 1) reveals a significant ($p < 0.0001$) positive correlation between the levels of IL-12p70, IL-13, IL-16, IL-1β, IL-1α, IL-6, IL-8, and TNF-α levels and the quantity of particles in the ABS and PC emissions sample medium. Details of cytokines/chemokines changes are given in Supplemental Table S4.

4. Discussion

The toxicity evaluation of emissions generated during 3-D printing is essential. The widespread use of this emerging technology in industries, along with the lack data on health effects available to consumers in homes and schools, highlights a knowledge gap, which must be filled.

This study sought to evaluate the cellular toxicity of emissions generated from a commercially available 3-D printer, while operating with PC or ABS filaments. Total emissions were collected during printing a 1.5 h print job, which is equivalent to production of a small object. It is probable that not all particles emitted during extrusion of ABS or PC filament were present in the media exposed to cells because of losses in the chamber and the BioSamplers® as well as agglomeration in the media. Chamber wall losses occur but in our experience with this chamber the fraction of particles lost is on the order of 10^{-4} (Yi et al., 2016). Particle losses in the BioSampler® include internal losses (the fraction of particles collected in media that is aerosolized from the collection liquid, adheres to the samplers walls, and remains on the walls) which can be 30% (Han and Mainelis, 2012) and sampling inefficiency, which may exceed 90% in the 20 to 300 nm size range because small particles have insufficient inertia to be collected in media by the centrifugal collection motion in the sampler (Riemenschneider et al., 2010). Accounting for chamber and BioSampler® losses, we estimate that less than 25% of emitted particles were collected in the SABM™ media. However, this value is likely an underestimate because the number of airborne particles that formed agglomerates in the media after being trapped in media but prior to determination of colloidal
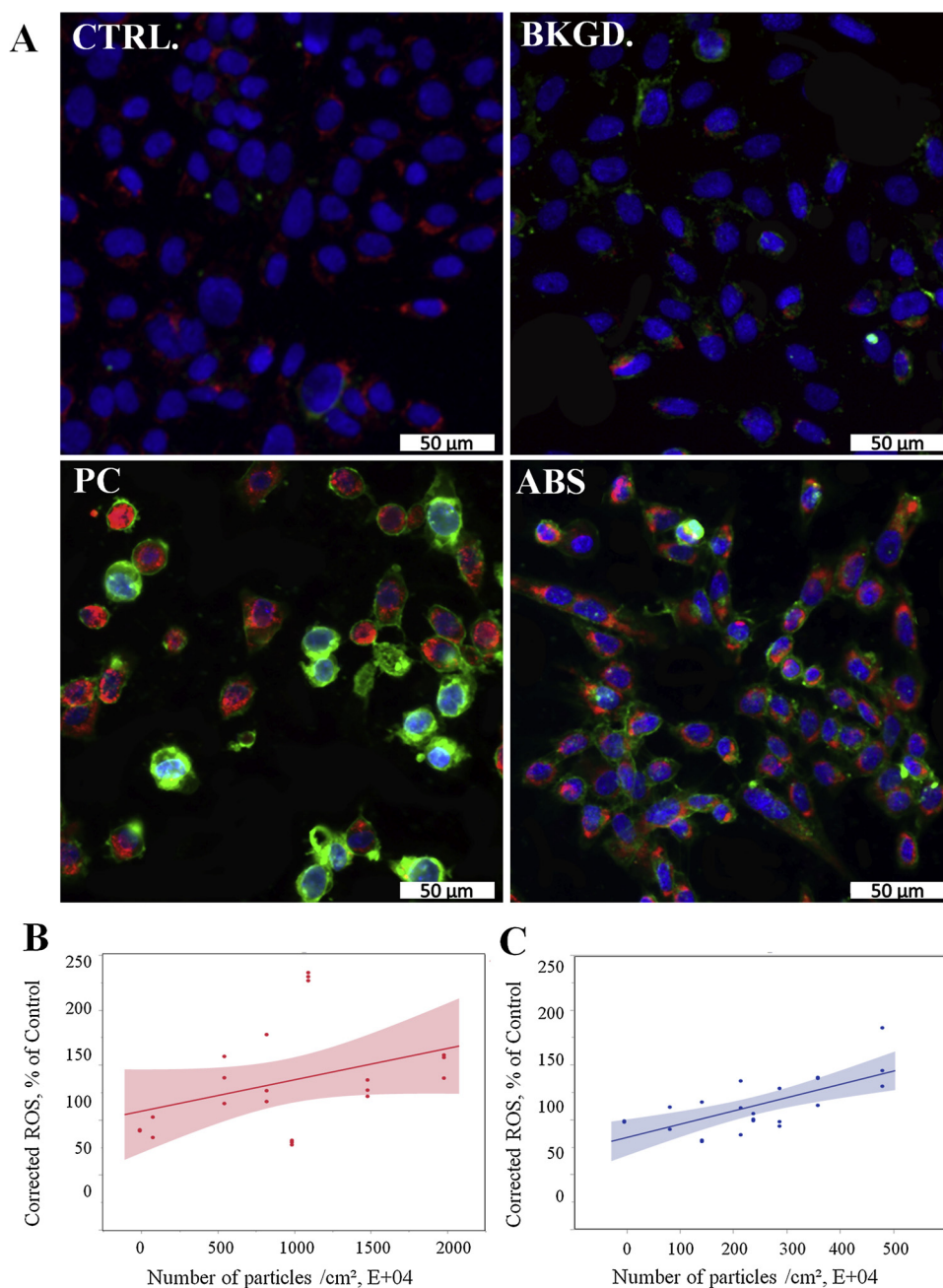
Fig. 5. ROS production following exposure to 3-D printer-emitted particles collected in the cell culture medium. SAEC were stained with a cocktail consisting of 5 μM CellROX™ Deep Red reagent, 5 μg/mL of CellMask™ Orange plasma membrane stain, and 1 μM Hoechst 33342 fluorescent nuclear stain. (A) Representative confocal images of untreated cells, and cells exposed to background, PC, and ABS collected emissions for 24 h. Quantitative ROS levels of PC (B) and ABS (C) using high content screening. Magnification at 20× and scale bars are at 50 μm for all images. Experiments were performed in three independent experiments with n = 6 replicates each. The regressions lines illustrate a significantly (p < 0.0001) increased dose-response relationship between ROS production and the numbers of the PC and ABS 3-D printer-emitted particles. The shaded area represents the 95% confidence interval around the regression line.

concentration is unknown.

This study revealed that the 3-D printer emissions collected in cell culture medium from PC and ABS filaments could be cytotoxic. This observation may be an effect of particle size. It has been well established that smaller particles cause more severe inflammation and oxidative stress than the larger particles at the same administered mass dose due to increased reactive surface area per particle (Duffin et al., 2007; Horie et al., 2012). Note that the size and morphology of particles in culture media that was delivered to cells likely differs from the characteristics of particles emitted into air during 3-D printing. In a prior study, extruding these ABS and PC filaments on the same printer released diffuse clusters of nanoscale polymer particles with geometric mobility mean sizes of 22.7 nm and 47.5 nm, respectively (Stefaniak et al., 2018). In culture media, the measured particle hydrodynamic diameters were about 170 to 200 nm (Table S2). It is important to clarify that the airborne particle size is the mobility diameter whereas the particle size in media is the hydrodynamic size. Hence, differences

in the basic measurement principle of each technique explain at least some of the observed deviation in particle size. Other factors contributing to the difference in particle size between the aerosol phase and the media include agglomeration in SABM™ if the particle surfaces are hydrophobic. Emitted particles from extrusion of ABS and PC are diffuse clusters with morphology similar to welding fume (Stefaniak et al., 2019) whereas the particles in culture medium were denser clusters (Fig. S2). Though changes in size and morphology were observed between the aerosol phase and particle in culture media, in humans, inhaled emissions would interact with lung airway-lining fluid and presumably be subject to interactions that alter particle size and morphology as well.

Metals may be present in filaments as constituents of plasticizers. Additionally, to enhance the printed object's aesthetic, structural, or functional properties, many types of additives and pigments, which may contain transition metals such as Cr, Fe, and Co, are added to the base polymer used to produce 3-D printer filaments. In this study, EDX
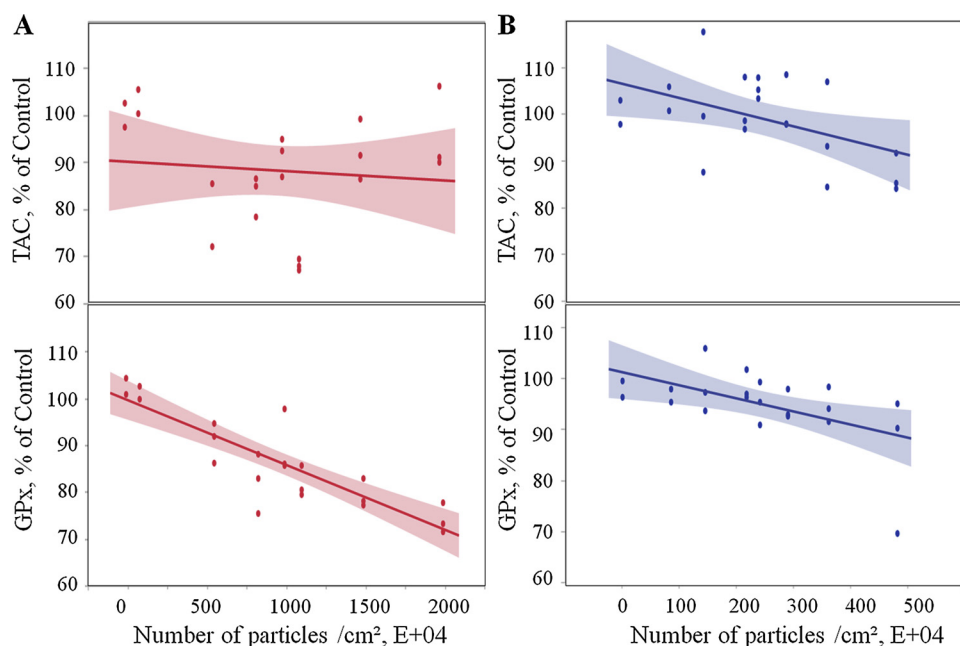
Fig. 6. Oxidative stress response following 3-D printer-emitted particles collected in the cell culture medium: total antioxidant capacity and glutathione peroxidase activity following exposure to PC (A) and ABS (B) emissions. Experiments were performed in three independent experiments with n = 3 replicates each. The regressions lines illustrate a significantly (p < 0.0001) decreased dose-response relationship between total antioxidant capacity and glutathione peroxidase activity and the numbers of the PC and ABS 3-D printer-emitted particles. The shaded area represents the 95% confidence interval around the regression line.

analysis showed that the main metals of health significance in the ABS and PC particles were Ni, Cr, and Fe. Aside from this study, to our knowledge, there is no information on the elemental composition of particles released during 3-D printing with PC filament. The presence of Ni, Cr, and Fe in particles emitted during 3-D printing with ABS were noted in this study as well as in other published studies (Stefaniak et al., 2017b; Steinle, 2016; Zontek et al., 2017), and might undergo redox-cycling (Fenton or Haber-Weiss reactions) and promote the production of ROS.

The induction of ROS and oxidative stress is one of the central proposed mechanisms of nanoparticle-induced toxicity (Nel et al., 2006). ROS are a collective term for the intermediates formed during oxidative metabolism, including both oxygen radicals and non-radical reactive oxygen derivatives. Cells normally maintain a low physiological level of ROS with antioxidant defense systems. Cellular systems are protected from ROS-induced cell injury by an array of defenses composed of various antioxidants with different functions. When levels of ROS overwhelm defense systems, either due to an increase in ROS production or a decrease antioxidant defense systems, oxidative stress can induce cellular macromolecule damage, including DNA, proteins and lipids (Touyz, 2012). In this study, we detected elevated production of ROS after exposure to medium containing emissions from printing with PC and ABS filaments. Similar findings were noted by Watson-Wright et al. (2017), who reported increased ROS production in SAEC exposed to the particulate matter released from the thermal decomposition of PC thermoplastic (Watson-Wright et al., 2017).

Oxidative stress is a biological process of an imbalance between the amount of ROS produced and the protective response of antioxidant defense systems. The measurement of antioxidant status can be used indirectly to assess oxidant stress (Palmieri and Sblendorio, 2007). Most of antioxidant enzymes are naturally induced upon the production of ROS *in vivo*, and the induction of antioxidant activities decrease or delays ROS-induced oxidative damage. Therefore, the measurement of antioxidant status not only indicates the status of the ROS production but also reflects the propensity of individuals to oxidative damage. In this study, collected PC and ABS emissions decreased TAC in exposed SAEC, indicating oxidative stress.

GPx is an antioxidant enzyme that catalyzes the reduction of hydrogen peroxide (H_2O_2) to water, and lipid peroxides to lipid alcohols *via* the oxidation of reduced glutathione (GSH) into its disulfide form (GSSH). In the absence of adequate GPx activity or glutathione levels,

H_2O_2 and lipid peroxides are not detoxified and may be converted to OH-radicals and lipid peroxyl radicals, respectively, which may result in oxidative stress-induced pathologies (Tabet and Touyz, 2007). We found that exposure of SAEC to medium containing PC or ABS emissions decreased total antioxidant capacity and GPx activity. Similarly, Watson-Wright et al. (2017) reported that released particulate matter from the thermal decomposition of PC thermoplastic caused a reduction in GSH levels in SAEC (Watson-Wright et al., 2017). Additionally, exposure to the products of oxidative thermal degradation of ABS caused a decrease of GSH and impairment of membrane integrity in isolated rat hepatocytes (Zitting and Heinonen, 1980).

The production of ROS and oxidative stress has been implicated in triggering and modulating apoptosis (Buttke and Sandstrom, 1994). In this study, increased apoptosis in SAEC was detected after exposure to PC or ABS emitted-particles collected in cell culture medium, which could be caused by the impairment of cellular redox homeostasis (Cazanave et al., 2007; Thompson and Franklin, 2010). Similarly, Watson-Wright et al. (Watson-Wright et al., 2017) demonstrated that the released particulate matter from the thermal decomposition of PC thermoplastic caused a reduction in mitochondrial membrane potential in SAEC, which could suggest a link between the disruption of intracellular redox homeostasis and the stimulation of mitochondrial apoptotic pathway. Additionally, we found that PC and ABS emissions collected in cell culture medium induced necrosis in SAEC. Recent studies found that some components of the apoptotic signaling pathway, such as the BH3-only protein (Bmf), are also crucial in the necrotic pathogenesis (Hitomi et al., 2008). Several studies showed that apoptosis and necrosis are closely linked to each other (Kaiser et al., 2011; Oberst et al., 2011). The apoptotic process may proceed to an autolytic necrotic outcome called secondary necrosis (Silva, 2010).

In an experimental exposure study in healthy human volunteers that investigated acute health effects of 3-D printing using high ultrafine particle-emitting ABS *vs* low-emitting polylactic acid (PLA) filaments, after 1 h post inhalation exposure, Gumperlein et al. (Gumperlein et al., 2018) found no acute effect on inflammatory markers in nasal secretions and urine. In our *in vitro* study, cellular exposure to medium containing emissions from 3-D printing with PC increased the production of pro-inflammatory cytokines, such as IL-1β, IL-1α, IL-6, IL-12(p70), IL-8, IL-13, IL-16, and TNF-α in SAEC. In contrast, medium containing ABS emissions only increased the production of IL-13. Further, these findings were correlated with increased production of ROS
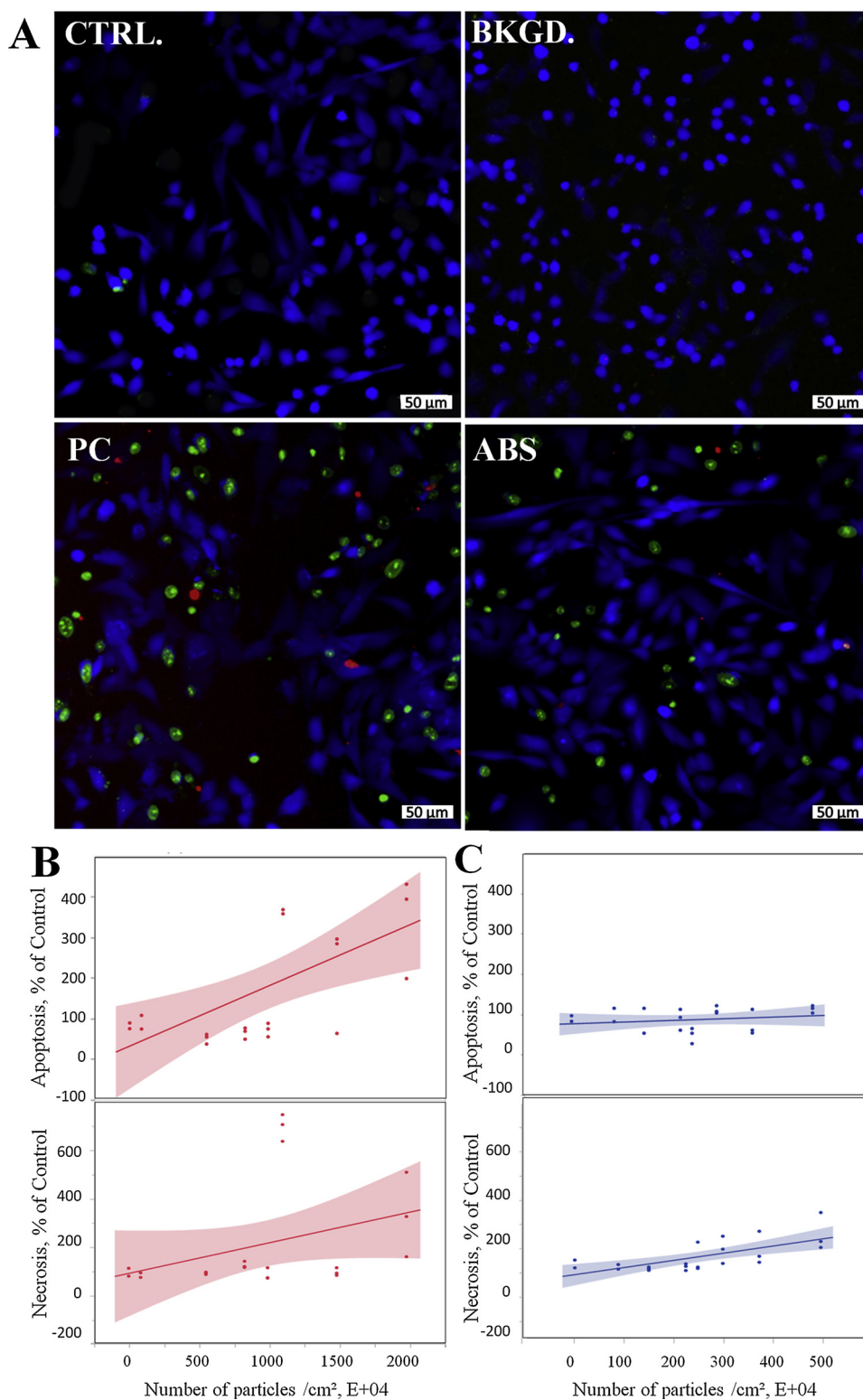
Fig. 7. 3-D printer-emitted particles collected in the cell culture medium increase apoptosis and necrosis. SAEC were stained with a cocktail consisting of 2 μL of Apopxin™ Red apoptosis stain, 1 μL of 200X Nuclear Green™ DCS1 necrotic stain, and 1 μL of CytoCalcein™ Violet 450 cytoplasmic stain. (A) Representative confocal images of untreated cells, and cells exposed to background, PC, and ABS collected emissions for 24 h. Quantitative apoptosis and necrosis analysis of PC (B) and ABS (C) using high content screening image analysis. Magnification at 10× and scale bars are at 50 μm for all images. Experiments were performed in three independent experiments with n = 6 replicates each. The regressions lines illustrate a significantly (p < 0.0001) increased dose-response relationship between apoptotic or necrotic events and the numbers of the PC and ABS 3-D printer-emitted particles. The shaded area represents the 95% confidence interval around the regression line.

and higher occurrence of apoptosis and necrosis in PC emissions-exposed cells. Cytokines and chemokines are known to orchestrate the intricate network of interactions associated with inflammatory process (Turner et al., 2014), and play an essential role in the pathogenesis of lung fibrosis, asthma, and chronic obstructive pulmonary disease (Barnes, 2008, 2009; Keane, 2008; Rincon and Irvin, 2012). IL-1 is a central mediator of innate immunity and inflammation and is released from lung epithelial cells to induce inflammatory responses (Tracy et al., 2012). It was found that IL-1β and TNF-α mediate apoptosis

through disrupting normal mitochondrial function in human chondrocytes (Kim et al., 2010). Also, IL-1α can be released from cells during apoptosis or necrosis (Berda-Haddad et al., 2011; Carta et al., 2013; van de Veerdonk and Netea, 2013), alerting the immune system to general tissue damage and initiating a cascade of inflammatory cytokines and chemokines (Chen et al., 2007; Rider et al., 2011). IL-13 secretion plays a key role in many aspects of airway remodeling (Fichtner-Feigl et al., 2006; Wills-Karp et al., 1998; Zhu et al., 1999). Overproduction of IL-13 could be a response to inadequate epithelial

repair due to injury. Previous studies established overexpression of IL-13 by epithelial cells in response to exposure to diesel exhaust using an *in vivo* model (Pourazar et al., 2004). Whether inhalation of 3-D printer emissions triggers inflammatory signaling in humans is still unclear, and further studies using longer exposure times representative of workers are needed.

There are many types of thermoplastic filaments and 3-D printers on the market, it would be a hard task to evaluate all of them in this research study. Therefore, we focused on one printer and two widely used filaments, PC and ABS using a chamber emissions collection system. First, we would like to emphasize that it is not possible to generalize our results from a single printer and two types of filaments to cover all 3-D printing. Second, in this study, major organic compounds present in cell culture medium after 3-D printing were qualitatively identified using SPME/GC–MS. However, it is well known that organic compound emission rates can be on the order of tens to hundreds of micrograms per gram of extruded polymer (Azimi et al., 2016; Floyd et al., 2017; Stefaniak et al., 2017b). Hence, it is possible that not all emitted organic compounds were collected in the cell culture medium during 3-D printing. Third, any reactive chemical species generated may be lost or form new species that may not exist in the printer emissions due interaction with components of the culture medium. However, the inhaled emissions would interact with lung airway-lining fluid and presumably be subject to interactions as well. It is also possible that if the particles collected in medium exhibit aqueous solubility, those with greater solubility would more likely to go into solution or leach adsorbed constituents into the media. Fourth, when inhaled, organic compounds and particles with surface adsorbed organics might not solubilize at the same relative levels as direct exposure to the cells; again, there would be interaction of deposited contaminants with airway-lining fluid. Fifth, operation of 3-D printers with polymer feedstock simultaneously releases both particulate and organic compounds, making it difficult to disentangle their relative effects on the observed endpoints. Sixth, the proximity of the BioSamplers® to the printer are only representative of some workplace scenarios where the employee is near a printer so the amount of emissions collected are likely higher than in a room with ventilation or where an employee only routinely checks the progress of a print job. Finally, even performing repeat print runs of the same filament using the same 3-D printer does not yield exactly the same results each time in terms of number of particles or types and amounts of organic compounds. Hence, within and between study comparisons of toxicity endpoints will be challenging because of inherent printer variability.

In this study, we observed that the FFF 3-D printer emissions collected in culture medium induced increased production of ROS and expression of pro-inflammatory cytokines and chemokines, as well as apoptosis and necrosis. Based on our results, we believe that the toxicological profiles of PC and ABS emissions are different. However, due to the complexity of these two emissions and different ranges of the particle numbers generated, it is hard to give a conclusion of toxicity between PC and ABS emissions in SAEC at this time. We will address this issue in the future.

5. Conclusions

This study demonstrated that 1) FFF 3-D printing with PC filaments resulted in more particles in cell culture medium than ABS over a similar printing time; 2) exposure to 3-D printer emissions collected in media induced dose-dependent toxicity in SAEC; and 3) emissions collected in media induced ROS production and oxidative stress, increased apoptosis and necrosis, and stimulated secretion of inflammatory chemokines and cytokines. The potential relationship with the observed *in vitro* effects as well as with hazard and risk of the workplace activity will need further studies with an exhaustive quantitative assessment of the detected chemicals, *in vitro* testing with defined mixtures of the relevant chemicals.

Appendix A. Supplementary data

Supplementary material related to this article can be found, in the online version, at doi:https://doi.org/10.1016/j.toxlet.2019.09.013.

References

ASTM-D6670, 2013. ASTM D6670: Standard Practice for Full-scale Chamber Determination of Volatile Organic Emissions from Indoor Materials/Products. ASTM International, West Conshohocken, PA.

Azimi, P., Zhao, D., Pouzet, C., Crain, N.E., Stephens, B., 2016. Emissions of ultrafine particles and volatile organic compounds from commercially available desktop three-dimensional printers with multiple filaments. Environ. Sci. Technol. 50, 1260–1268.

Barnes, P.J., 2008. The cytokine network in asthma and chronic obstructive pulmonary disease. J. Clin. Invest. 118, 3546–3556.

Barnes, P.J., 2009. The cytokine network in chronic obstructive pulmonary disease. Am. J. Respir. Cell Mol. Biol. 41, 631–638.

Berda-Haddad, Y., Robert, S., Salers, P., Zekraoui, L., Farnarier, C., Dinarello, C.A., Dignat-George, F., Kaplanski, G., 2011. Sterile inflammation of endothelial cell-derived apoptotic bodies is mediated by interleukin-1alpha. Proc. Natl. Acad. Sci. U. S. A. 108, 20684–20689.

Buttke, T.M., Sandstrom, P.A., 1994. Oxidative stress as a mediator of apoptosis. Immunol. Today 15, 7–10.

Carta, S., Lavieri, R., Rubartelli, A., 2013. Different members of the IL-1 family come out in different ways: DAMPs vs. cytokines? Front. Immunol. 4, 123.

Cazanave, S., Berson, A., Haouzi, D., Vadrot, N., Fau, D., Grodet, A., Letteron, P., Feldmann, G., El-Benna, J., Fromenty, B., Robin, M.A., Pessayre, D., 2007. High hepatic glutathione stores alleviate Fas-induced apoptosis in mice. J. Hepatol. 46, 858–868.

Chambers, K.M., Mandavilli, B.S., Dolman, N.J., Janes, M.S., 2018. General staining and segmentation procedures for high content imaging and analysis. Methods Mol. Biol. 1683, 21–31.

Chen, C.J., Kono, H., Golenbock, D., Reed, G., Akira, S., Rock, K.L., 2007. Identification of a key pathway required for the sterile inflammatory response triggered by dying cells. Nat. Med. 13, 851–856.

de Almeida Monteiro Melo Ferraz, M., Henning, H.H.W., Ferreira da Costa, P., Malda, J., Le Gac, S., Bray, F., van Duursen, M.B.M., Brouwers, J.F., van de Lest, C.H.A., Bertijn, I., Kraneburg, L., Vos, P.L.A.M., Stout, T.A.E., Gadella, B.M., 2018. Potential health and environmental risks of three-dimensional engineered polymers. Environ. Sci. Technol. Lett. 5, 80–85.

Deng, Y., Cao, S.-J., Chen, A., Guo, Y., 2016. The impact of manufacturing parameters on submicron particle emissions from a desktop 3D printer in the perspective of emission reduction. Build. Environ. 104, 311–319.

Duffin, R., Tran, L., Brown, D., Stone, V., Donaldson, K., 2007. Proinflammogenic effects of low-toxicity and metal nanoparticles in vivo and in vitro: highlighting the role of particle surface area and surface reactivity. Inhal. Toxicol. 19, 849–856.

Fichtner-Feigl, S., Strober, W., Kawakami, K., Puri, R.K., Kitani, A., 2006. IL-13 signaling through the IL-13alpha2 receptor is involved in induction of TGF-beta1 production and fibrosis. Nat. Med. 12, 99–106.

Floyd, E.L., Wang, J., Regens, J.L., 2017. Fume emissions from a low-cost 3-D printer with various filaments. J. Occup. Environ. Hyg. 14, 523–533.

Gu, J., Wensing, M., Uhde, E., Salthammer, T., 2019. Characterization of particulate and gaseous pollutants emitted during operation of a desktop 3D printer. Environ. Int. 123, 476–485.

Gumperlein, I., Fischer, E., Dietrich-Gumperlein, G., Karrasch, S., Nowak, D., Jorres, R.A., Schierl, R., 2018. Acute health effects of desktop 3D printing (fused deposition modeling) using acrylonitrile butadiene styrene and polylactic acid materials: an experimental exposure study in human volunteers. Indoor Air 28, 611–623.

Han, T., Mainelis, G., 2012. Investigation of inherent and latent internal losses in liquid-based bioaerosol samplers. J. Aerosol Sci. 45, 58–68.

Hitomi, J., Christofferson, D.E., Ng, A., Yao, J., Degterev, A., Xavier, R.J., Yuan, J., 2008. Identification of a molecular signaling network that regulates a cellular necrotic cell death pathway. Cell 135, 1311–1323.

Horie, M., Fukui, H., Endoh, S., Maru, J., Miyauchi, A., Shichiri, M., Fujita, K., Niki, E., Hagihara, Y., Yoshida, Y., Morimoto, Y., Iwahashi, H., 2012. Comparison of acute oxidative stress on rat lung induced by nano and fine-scale, soluble and insoluble metal oxide particles: NiO and TiO2. Inhal. Toxicol. 24, 391–400.

House, R., Rajaram, N., Tarlo, S.M., 2017. Case report of asthma associated with 3D printing. Occup. Med. (Lond.) 67, 652–654.

ISO.28360, 2007. ISO. 28360: Information Technology — Office Equipment — Determination of Chemical Emission Rates From Electronic Equipment. International Organization for Standardization, Geneva, Switzerland.

Kaiser, W.J., Upton, J.W., Long, A.B., Livingston-Rosanoff, D., Daley-Bauer, L.P., Hakem, R., Caspary, T., Mocarski, E.S., 2011. RIP3 mediates the embryonic lethality of caspase-8-deficient mice. Nature 471, 368–372.

Keane, M.P., 2008. The role of chemokines and cytokines in lung fibrosis. Eur. Respir. Rev. 17, 151.

Kim, J., Xu, M., Xo, R., Mates, A., Wilson, G.L., Pearsall, A.W., Grishko, V., 2010. Mitochondrial DNA damage is involved in apoptosis caused by pro-inflammatory cytokines in human OA chondrocytes. Osteoarthr. Cartil. 18, 424–432.

Kim, Y., Yoon, C., Ham, S., Park, J., Kim, S., Kwon, O., Tsai, P.J., 2015. Emissions of nanoparticles and gaseous material from 3D printer operation. Environ. Sci. Technol. 49, 12044–12053.

Lodovici, M., Bigagli, E., 2011. Oxidative stress and air pollution exposure. J. Toxicol. 2011, 487074.

Macdonald, N.P., Zhu, F., Hall, C.J., Reboud, J., Crosier, P.S., Patton, E.E., Wlodkowic, D., Cooper, J.M., 2016. Assessment of biocompatibility of 3D printed photopolymers using zebrafish embryo toxicity assays. Lab Chip 16, 291–297.

MarketResearchEngine, 2018. https://www.marketresearchengine.com/industrial-3D-printing-market.

Moylan, S., Slotwinski, J., Cooke, A., Jurrens, K., Donmez, M.A., 2014. An additive manufacturing test artifact. J. Res. Inst. Stand. Technol. 119, 429–459.

Nel, A., Xia, T., Mädler, L., Li, N., 2006. Toxic potential of materials at the nanolevel. Science 311, 622–627.

Oberst, A., Dillon, C.P., Weinlich, R., McCormick, L.L., Fitzgerald, P., Pop, C., Hakem, R., Salvesen, G.S., Green, D.R., 2011. Catalytic activity of the caspase-8-FLIP(L) complex inhibits RIPK3-dependent necrosis. Nature 471, 363–367.

Oskui, S.M., Diamante, G., Liao, C., Shi, W., Gan, J., Schlenk, D., Grover, W.H., 2016. Assessing and reducing the toxicity of 3D-printed parts. Environ. Sci. Technol. Lett. 3, 1–6.

Palmieri, B., Sblendorio, V., 2007. Oxidative stress tests: overview on reliability and use. Part II. Eur. Rev. Med. Pharmacol. Sci. 11, 383–399.

Piao, C.Q., Liu, L., Zhao, Y.L., Balajee, A.S., Suzuki, M., Hei, T.K., 2005. Immortalization of human small airway epithelial cells by ectopic expression of telomerase. Carcinogenesis 26, 725–731.

Pourazar, J., Frew, A.J., Blomberg, A., Helleday, R., Kelly, F.J., Wilson, S., Sandstrom, T., 2004. Diesel exhaust exposure enhances the expression of IL-13 in the bronchial epithelium of healthy subjects. Respir. Med. 98, 821–825.

Rider, P., Carmi, Y., Guttman, O., Braiman, A., Cohen, I., Voronov, E., White, M.R., Dinarello, C.A., Apte, R.N., 2011. IL-1α and IL-1β recruit different myeloid cells and promote different stages of sterile inflammation. J. Immunol. 187, 4835.

Riemenschneider, L., Woo, M.H., Wu, C.Y., Lundgren, D., Wander, J., Lee, J.H., Li, H.W., Heimbuch, B., 2010. Characterization of reaerosolization from impingers in an effort to improve airborne virus sampling. J. Appl. Microbiol. 108, 315–324.

Rincon, M., Irvin, C.G., 2012. Role of IL-6 in asthma and other inflammatory pulmonary diseases. Int. J. Biol. Sci. 8, 1281–1290.

Silva, M.T., 2010. Secondary necrosis: the natural outcome of the complete apoptotic program. FEBS Lett. 584, 4491–4499.

Stabile, L., Scungio, M., Buonanno, G., Arpino, F., Ficco, G., 2017. Airborne particle emission of a commercial 3D printer: the effect of filament material and printing temperature. Indoor Air 27, 398–408.

Stefaniak, A.B., Bowers, L.N., Knepp, A.K., Luxton, T.P., Peloquin, D.M., Baumann, E.J., Ham, J.E., Wells, J.R., Johnson, A.R., LeBouf, R.F., Su, F.C., Martin, S.B., Virji, M.A., 2019. Particle and vapor emissions from vat polymerization desktop-scale 3-dimensional printers. J. Occup. Environ. Hyg. 1–13.

Stefaniak, A.B., Bowers, L.N., Knepp, A.K., Virji, M.A., Birch, E.M., Ham, J.E., Wells, J.R., Qi, C., Schwegler-Berry, D., Friend, S., Johnson, A.R., Martin Jr., S.B., Qian, Y.,

LeBouf, R.F., Birch, Q., Hammond, D., 2018. Three-dimensional printing with nano-enabled filaments releases polymer particles containing carbon nanotubes into air. Indoor Air 28, 840–851.

Stefaniak, A.B., LeBouf, R.F., Duling, M.G., Yi, J., Abukabda, A.B., McBride, C.R., Nurkiewicz, T.R., 2017a. Inhalation exposure to three-dimensional printer emissions stimulates acute hypertension and microvascular dysfunction. Toxicol. Appl. Pharmacol. 335, 1–5.

Stefaniak, A.B., LeBouf, R.F., Yi, J., Ham, J., Nurkewicz, T., Schwegler-Berry, D.E., Chen, B.T., Wells, J.R., Duling, M.G., Lawrence, R.B., Martin Jr., S.B., Johnson, A.R., Virji, M.A., 2017b. Characterization of chemical contaminants generated by a desktop fused deposition modeling 3-dimensional Printer. J. Occup. Environ. Hyg. 14, 540–550.

Steinle, P., 2016. Characterization of emissions from a desktop 3D printer and indoor air measurements in office settings. J. Occup. Environ. Hyg. 13, 121–132.

Stephens, B., Azimi, P., El Orch, Z., Ramos, T., 2013. Ultrafine particle emissions from desktop 3D printers. Atmos. Environ. 79, 334–339.

Tabet, F., Touyz, R.M., 2007. Chapter 30 - reactive oxygen species, oxidative stress, and vascular biology in hypertension. In: Lip, G.Y.H., Hall, J.E. (Eds.), Comprehensive Hypertension. Mosby, Philadelphia, pp. 337–347.

Thompson, J.A., Franklin, C.C., 2010. Enhanced glutathione biosynthetic capacity promotes resistance to As3 + -induced apoptosis. Toxicol. Lett. 193, 33–40.

Touyz, R.M., 2012. Chapter 69 - reactive oxygen species and oxidative stress. In: Robertson, D., Biaggioni, I., Burnstock, G., Low, P.A., Paton, J.F.R. (Eds.), Primer on the Autonomic Nervous System (Third Edition). Academic Press, San Diego, pp. 335–338.

Tracy, E.C., Bowman, M.J., Henderson, B.W., Baumann, H., 2012. Interleukin-1alpha is the major alarmin of lung epithelial cells released during photodynamic therapy to induce inflammatory mediators in fibroblasts. Br. J. Cancer 107, 1534–1546.

Turner, M.D., Nedjai, B., Hurst, T., Pennington, D.J., 2014. Cytokines and chemokines: At the crossroads of cell signalling and inflammatory disease. Biochim. Biophys. Acta 1843, 2563–2582.

van de Veerdonk, F.L., Netea, M.G., 2013. New insights in the immunobiology of IL-1 family members. Front. Immunol. 4, 167.

Vance, M.E., Pegues, V., Van Montfrans, S., Leng, W., Marr, L.C., 2017. Aerosol emissions from fuse-deposition modeling 3D printers in a chamber and in real indoor environments. Environ. Sci. Technol. 51, 9516–9523.

Watson-Wright, C., Singh, D., Demokritou, P., 2017. Toxicological implications of released particulate matter during thermal decomposition of nano-enabled thermoplastics. NanoImpact 5, 29–40.

Wills-Karp, M., Luyimbazi, J., Xu, X., Schofield, B., Neben, T.Y., Karp, C.L., Donaldson, D.D., 1998. Interleukin-13: central mediator of allergic asthma. Science 282, 2258–2261.

Wojtyła, S., Klama, P., Baran, T., 2017. Is 3D printing safe? Analysis of the thermal treatment of thermoplastics: ABS, PLA, PET, and nylon. J. Occup. Environ. Hyg. 14, D80–D85.

Xia, T., Kovochich, M., Nel, A., 2006. The role of reactive oxygen species and oxidative stress in mediating particulate matter injury. Clin. Occup. Environ. Med. 5, 817–836.

Xu, Y., Wu, X., Guo, X., Kong, B., Zhang, M., Qian, X., Mi, S., Sun, W., 2017. The boom in 3D-printed sensor technology. Sensors (Basel) 17.

Yi, J., LeBouf, R.F., Duling, M.G., Nurkiewicz, T., Chen, B.T., Schwegler-Berry, D., Virji, M.A., Stefaniak, A.B., 2016. Emission of particulate matter from a desktop three-dimensional (3D) printer. J. Toxicol. Environ. Health A 79, 453–465.

Zhang, Q., Wong, J., Davis, A., Black, M., Weber, R., 2017. Characterization of particle emissions from consumer fused deposition modeling 3D printers. Aerosol Sci. Technol. 51, 1275–1286.

Zhou, Y., Kong, X., Chen, A., Cao, S., 2015. Investigation of ultrafine particle emissions of desktop 3D printers in the clean room. Procedia Eng. 121, 506–512.

Zhu, Z., Homer, R.J., Wang, Z., Chen, Q., Geba, G.P., Wang, J., Zhang, Y., Elias, J.A., 1999. Pulmonary expression of interleukin-13 causes inflammation, mucus hypersecretion, subepithelial fibrosis, physiologic abnormalities, and eotaxin production. J. Clin. Invest. 103, 779–788.

Zitting, A., Heinonen, T., 1980. Decrease of reduced glutathione in isolated rat hepatocytes caused by acrolein, acrylonitrile, and the thermal degradation products of styrene copolymers. Toxicology 17, 333–341.

Zontek, T.L., Ogle, B.R., Jankovic, J.T., Hollenbeck, S.M., 2017. An exposure assessment of desktop 3D printing. J. Chem. Health Saf. 24, 15–25.